Scale Effect on CFRP Strengthening of Infilled Reinforced Concrete Frames

Emre Akin, Erdem Canbay, Baris Binci, Güney Özcebe

Journal of Advanced Concrete Technology, volume 13 (2015), pp. 355-366

Scientific paper

Scale Effect on CFRP Strengthening of Infilled Reinforced Concrete Frames

Emre Akın[1*], Erdem Canbay[2], Barış Binici[2] and Güney Özcebe[3]

Received 18 March 2015, accepted 7 July 2015 doi:10.3151/jact.13.355

Abstract

The diagonal application of Carbon Fiber-Reinforced Polymer fabrics on hollow clay tile infill walls has been qualified as an efficient rehabilitation method for deficient reinforced concrete frames. However, majority of the experimental studies were conducted on 1/3-scaled RC frames and the effect of specimen scaling has not been questioned. In the current study, the results of an experimental campaign on 1/2-scaled RC frames are presented. Test specimens are grouped in two series having two different aspect ratios. In each series, there are two RC frames having hollow clay tile infill walls with/without CFRP reinforcement. The results of 1/2-scaled specimens are compared with the experimental results obtained from 1/3-scaled frames. In addition, the numerical model which were developed by the authors for 1/3-scaled frames are employed for modeling 1/2-scaled specimens and the results were assessed by comparing with the test results.

1. Introduction

The application of diagonal Carbon Fiber-Reinforced Polymer (CFRP) fabrics on the existing hollow clay tile (HCT) infill walls of deficient reinforced concrete (RC) frames have been investigated in a number of studies (Almusallam and Al-Salloum 2007; Ersoy *et al*. 2003; Kobayashi 2007; Luccioni and Rougier 2011; Mahmood and Ingham 2011; Nateghi-Elahi and Dehghani 2008; Özcebe *et al*. 2004; Özcebe *et al*. 2006; Özden and Akgüzel 2006; Saatcioglu *et al*. 2005; Spyrakos *et al*. 2012; Yüksel *et al*. 2009). Based on the result of these studies, the design guidelines of the rehabilitation method that relies on the use of CFRP application on HTCs have already been established (Binici *et al*. 2007; Tan *et al*. 2009; Turkish Earthquake Code 2007). The early experimental studies have been conducted on 1/3-scale RC frames mostly due to limited laboratory facilities (Ersoy *et al*. 2003; Özcebe *et al*. 2004). In the literature there were few studies where 1/2-scaled RC frames were considered (Saatcioglu *et al*. 2005; Erol *et al*. 2008; Yüksel *et al*. 2006). None of these studies, however, focused on the effect of scale difference on the observed behavior of the test specimens. The objective of this study is to compare the structural engineering parameters from reinforced concrete frame tests with two different scales. In addition, the numerical simulation results are further validated by using the test results.

[1]Assistant Professor, Department of Civil Engineering, Adnan Menderes University, Aydın, Turkey.
*Corresponding author, *E-mail*: eakin@adu.edu.tr
[2]Professor, Department of Civil Engineering, Middle East Technical University, Ankara, Turkey.
[3]Professor, Department of Civil Engineering, TED University, Ankara, Turkey.

In the current article, the experimental and numerical studies conducted on 1/2-scale RC frames with or without strengthened HCT infill walls are presented. The material and specimen specifications, and the test setup are introduced. The observed behaviors of specimens are explained. Test results are provided in terms of strength, stiffness, ductility and energy dissipation characteristics. These results are compared with the former experimental results obtained from 1/3-scaled RC frames. In the last part, the pushover analyses results of the numerical model of CFRP strengthened RC frames are given in comparison with the experimental curves.

2. Experimental program

2.1 Test specimens

Four 1/2-scaled specimens were tested in two series, namely Series-L and Series-N. The aspect (height to width) ratio of frames in Series-L was 0.60 in both stories, so as to represent the frames with squat infill walls. In order to represent the frames with narrow infill walls, the aspect ratios of Series-N frames were chosen to be 2.30 and 1.72 in the first and second stories, respectively. The higher aspect ratio (i.e. higher columns) in the first story reflects soft story deficiency in these frames. The specimens are illustrated in **Fig. 1**. In each series, the first specimen was a reference frame with non-strengthened HCT infill walls. Whereas the second specimen was strengthened by the method explained in this study. The properties and design details of all test specimens are given in **Table 1**.

The two-story and one-bay specimens were designed to represent 1/2-scale model of non-ductile frame which have strong beams and weak columns. The design and construction of the specimens intentionally lead to a deficient frame having the common structural deficiencies of RC buildings. The plain bars were used for both

Table 1 Properties and design details of the test specimens.

Specimen	Type	Aspect Ratio	f_c' (MPa)	f_m' * (MPa)	f_{in} * (MPa)
LREF-1/2	Infilled	0.60 (both stories)	19.8	5.3	15.3
LSTR-1/2	Strength.		20.7	5.6	15.3
NREF-1/2	Infilled	2.30 (1st story)	19.3	5.3	15.3
NSTR-1/2	Strength.	1.74 (2nd story)	20.4	5.6	15.3

* f_m' and f_{in} are the compressive strength of the mortar and infill material, respectively.

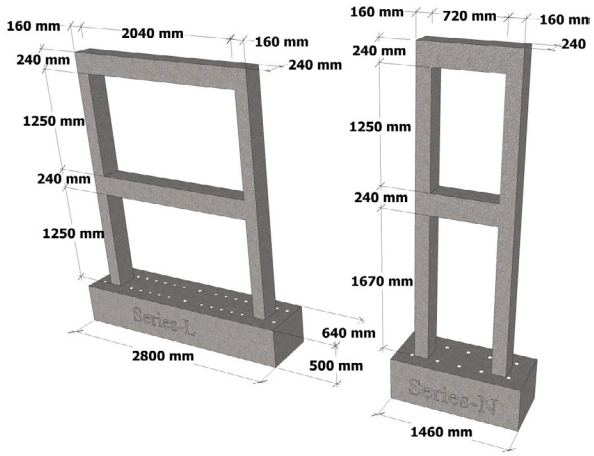

Fig. 1 Dimensions of the 1/2-scaled test specimens.

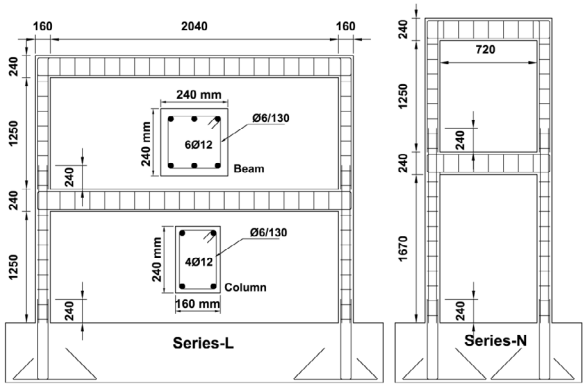

Fig. 2 Reinforcement details of 1/2-scaled test specimens.

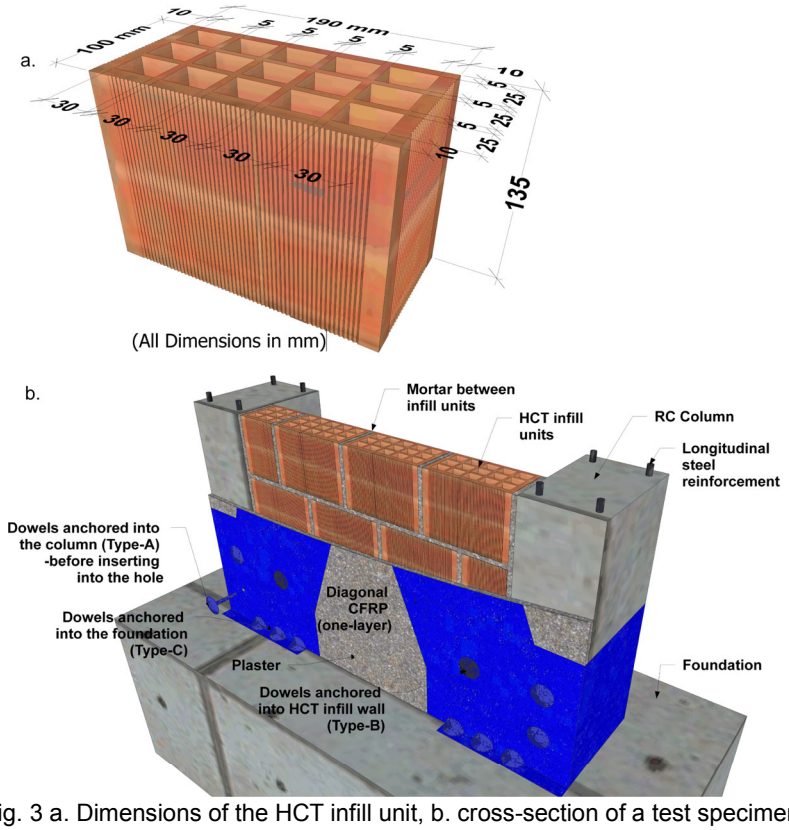

Fig. 3 a. Dimensions of the HCT infill unit, b. cross-section of a test specimen.

transverse and longitudinal reinforcement. The transverse reinforcement was improper (i.e. plain bars with 90° hooks) and insufficient (i.e. the spacing satisfies neither Turkish Earthquake Code (2007) nor American Concrete Institute (ACI Committee 318 2005) requirements). The column longitudinal bars were lapped at each story level over a length of 240 mm. This lap-splice length corresponds to 20 times the bar diameter which is half of what is required by Turkish Earthquake Code (2007). The reinforcement detailing of the frames are presented in **Fig. 2**. The average concrete compressive strength was 20 MPa (**Table 1**).

Table 2 Material properties of the reinforcing steel, CFRP and epoxy.

Material	Type	f_y (MPa)	f_u (MPa)	E (MPa)	Weight per unit area (g/m^2)	Effective thickness (mm)
Steel	Stirrup	340	474	200000	N/A	N/A
	Longitudi.	380	510	200000	N/A	N/A
CFRP		N/A	3430	230000	300	0.166
Epoxy		N/A	50	3500	N/A	N/A

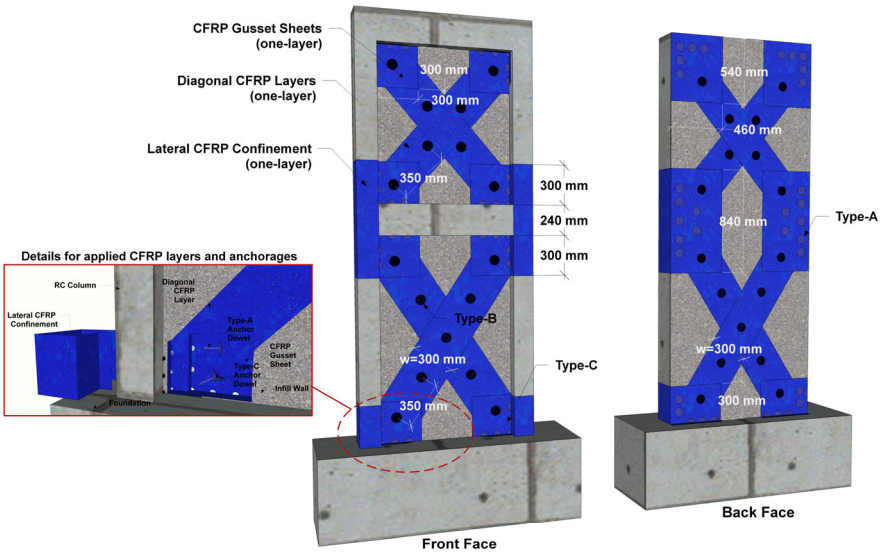

Fig. 4 CFRP strengthening applied on 1/2-scaled Series-N frame.

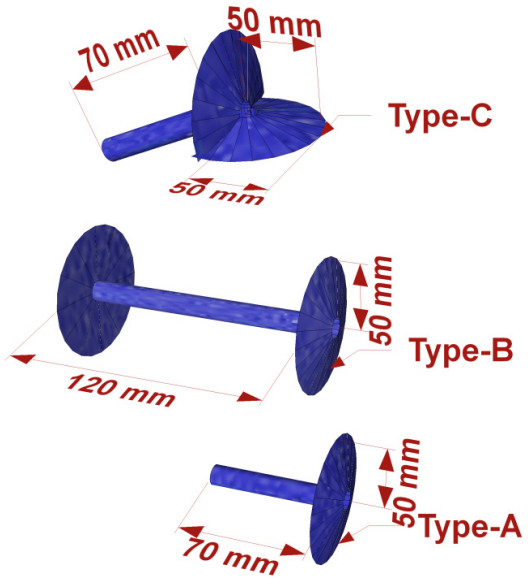

Fig. 5 The three different types of anchor dowels used in CFRP strengthening.

The cross-sectional dimensions of the columns and beams were 160 mm x 240 mm and 240 mm x 240 mm, respectively. The 12-mm diameter plain bars were used for the longitudinal reinforcement of the columns and beams as shown in **Fig. 2**. The confinement of all members was provided by 6 mm diameter stirrups which were spaced at 130 mm. The properties of the reinforcing steel are provided in **Table 2**.

The infill units of the frames were produced by cutting the conventional HCT's into two pieces, such that they had a void ratio of 59 percent (**Fig. 3a**). The net compressive strength of infill units (i.e. excluding voids of the tile) was 15.3 MPa. The infill walls were constructed and about 10 mm thick plaster was applied on both faces of the walls by a professional mason. The applied mortar and plaster had a compressive strength of approximately 5.5 MPa (**Table 1**). The arrangement of the HCT units and plaster are illustrated in **Fig. 3b**.

One specimen in both series was strengthened by means of CFRP sheets (**Fig. 4**). This figure shows the strengthening scheme of Series-N specimens. The fastening of one-layer CFRP sheet, having a width of 300 mm, along each diagonal of infill walls constitutes the major part of strengthening. These CFRP fabrics were extended to RC frame members and anchored both to the infill and frame in order to prevent early de-bonding. The anchorage was provided by means of dowels which were manufactured by rolling and binding 100 mm width CFRP strips around guide wires. The holes with a diameter of 10 mm were drilled throughout the infill walls and around 70 mm into the RC frame members. After cleaning the dust and injecting epoxy, the anchor dowels were inserted into these holes. The free ends of the dowels sticking out of the holes were splayed over the underlying CFRP. Type-A, Type-B and Type-C anchor dowels which were prepared in the same manner and inserted into the RC frame members, HCT infill walls and foundation, respectively are illustrated in **Fig. 5**. Also, a Type-A anchor dowel right before insertion into the hole is presented in **Fig. 3b**. The lap-splice regions of the columns at the base of each story were confined with one-layer of horizontally oriented CFRP fab-

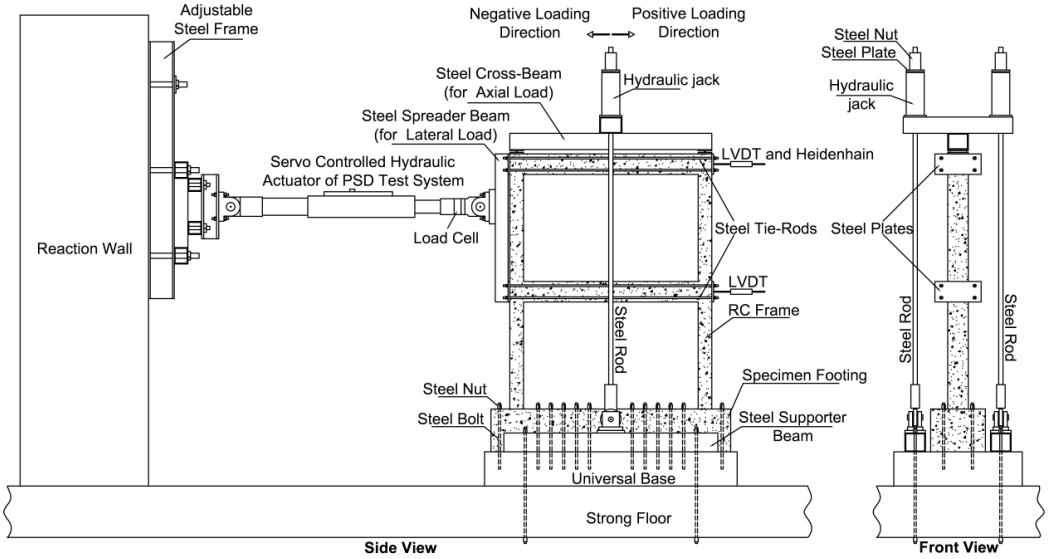

Fig. 6 Test setup for 1/2-scaled test specimens.

rics over a height of 300 mm (**Fig. 4**). These regions were wrapped after rounding the corners of the columns in order to avoid stress concentrations and possible premature CFRP rupture. The corners of the infill walls were further covered with square CFRP gusset sheets to provide more uniform stress distribution between diagonal CFRP and RC frame. Another reason of covering these regions was to prevent excessive early damage at these regions.

2.2 Test setup

The reversed cyclic lateral loading that simulates seismic actions was applied for all specimens. These lateral loads were generated by the servo-controlled hydraulic actuators with a capacity of 500 kN. In order to be compatible with the previous test group (Akın *et al*. 2011), it was used for the generation of static reversed cyclic loads. A steel spreader beam was used in order to split the total load at each story-level, such that two thirds of the lateral load was transferred to the second floor and the remaining part is applied on the first story. The actuator was supported by a reaction wall. The hinge connections were provided at both ends of the actuator in order to prevent a column sway mechanism. In addition to the built-on load cell the actuators, another load cell having a capacity of 500 kN was also mounted on the actuator by an adaptor in order to synchronize the data collected by a separate data acquisition system. The test setup is presented in **Fig. 6**.

The specimens were subjected to a constant axial load (i.e. ten percent of the nominal axial capacity of the columns) throughout the tests. The axial load was applied through the high strength steel rods post-tensioned by two hydraulic jacks on both sides of the specimen. This load was transmitted by the steel rods to the steel beam located at the top of the specimens and distributed equally on the columns by means of this spreader beam (**Fig. 6**). It should be noted that the steel-rods were hinge-connected to the strong-floor of the laboratory at the bottom. The hinge-connection allows rotational movements reflecting the lateral displacements experienced by the specimen.

Lateral bracing frames (not shown in **Fig. 6**) were provided on either side of the test specimen to prevent the out-of-plane motion and to keep the specimen in the plane-of-loading. An electronic data acquisition system with control-feedback was utilized in order to record the applied loads, in plane-displacements and strains. Strain gage based linear variable differential transformers (LVDT's) were used for measuring both story lateral frame displacements and shear deformations of infill walls. Additionally, the applied lateral load and displacements were also monitored by the built-in load cell and displacement transducer (i.e. Heidenhain with 500 mm stroke capacity) of the PSD system. The recordings of two data acquisition systems provided a confirmation for the results.

3. Test results

The observed behavior of the test frames is summarized regarding significant damage states. The failure pattern of the test specimens are shown in **Fig. 7**. The roof drift ratio (i.e. RDR, roof displacement over height of the frame) and inter-story drift ratio (i.e. IDR, first story displacement over height of the first story) values corresponding to each damage state are indicated. The hysteretic base shear vs. first story and roof displacement curves of the test frames are presented in **Figs. 8** and **9**, respectively. The RDR and IDR values are also indicated in **Figs. 8** and **9**, respectively.

3.1 Series-L tests

In both tests, the first cracks were in the form of flexural cracks on the first story columns. These initial cracks were observed at about 0.17% RDR and 0.25% IDR.

Fig. 7 Failure pattern of the test frames (a) LREF-1/2, (b) LSTR-1/2, (c) NREF-1/2 and (d) NSTR-1/2.

This corresponds to the onset of elastic-plastic transition zone on the hysteretic curve. This was followed by diagonal cracks on the HCT infill wall and separation at the frame-infill boundary. These cracks which state a compression strut formation along the diagonal of HCT infill walls took place at 0.34% and 1.00% RDR's for LREF-1/2 and LSTR-1/2, respectively. The corresponding IDR values were 0.40% and 1.30% for LREF-1/2 and LSTR-1/2, respectively. These values state that strut formation had been observed before the ultimate load capacity was reached. In specimen LREF-1/2, the crushing of first story infill wall at the corners lead to wide shear cracks at the beam-column joints (i.e. short column formation in **Fig. 7a**). In LSTR-1/2, the anchor dowels which connect CFRP cross-overlay sheets to the RC frame at the back face failed at about 1.40% RDR and 2.25% IDR. After anchorage failures, the diagonal CFRP sheets experienced de-bonding under compression and ruptured in the following half cycle under high tensile stresses (i.e. at 1.80% RDR and 3.00% IDR). The contribution of CFRP reinforcement ceased after this stage, which correspond to more than 20% decrease in the lateral load capacity. The wide shear cracks at the beam-column joints and crushing of concrete stated failure of the frame (**Fig. 7b**).

3.2 Series-N tests

Similar to Series-L frame tests, the initial flexural cracks developed on the first story columns at about 0.17% RDR and 0.20 IDR. This states the initiation of elastic-plastic transition zone on the hysteretic curve. Consequently, the separation was observed in specimen NREF-1/2 between the HTC infill wall and the frame at a RDR of 0.75% and IDR of 1.00%. However, instead of formation of a separation crack at the HCT infill wall – footing interface, a horizontal crack formed across the HCT infill wall at nearly 300 mm above the base. Subsequently, the infill wall separated from the first-story column in the vertical direction above this level, which is just over the lap-splice region (**Fig. 7c**). This observation indicated that the diagonal strut formation may not be observed properly in the case of narrow frames. In specimen NSTR-1/2, such a separation of the frame and HCT infill wall was observed at the RDR of 1.10% and IDR of 1.20%. The damage concentrated at the lap splice regions of first story columns at the final stage of both tests. The excessive damage and crushing of cover concrete at these regions marked the end-of-test for specimen NREF-1/2.

In the case of reinforced specimen, after the rupture of diagonal CFRP on the infill, the damage intensified at the lap splice regions also in specimen NSTR-1/2 (**Fig. 7d**). It should be noted that the damage on the infill walls of Series-N frames were not as significant as those in Series-L specimens. The test was terminated after the rupture of lateral CFRP sheets at the lap-splice regions and diagonal CFRP at the back face of specimen at about 3.60% RDR and 4.40% IDR.

4. Discussion of test results

The strength, initial stiffness, ductility and energy dissipation capacity of the specimens are presented and discussed in a comparative manner. The envelope curves

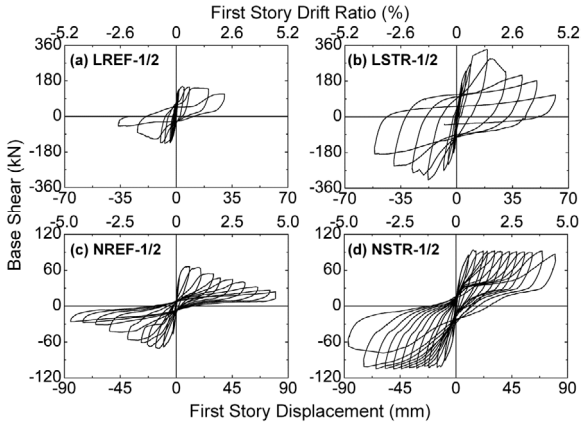

Fig. 8 Hysteretic base shear vs. first story displacement (drift ratio) curves.

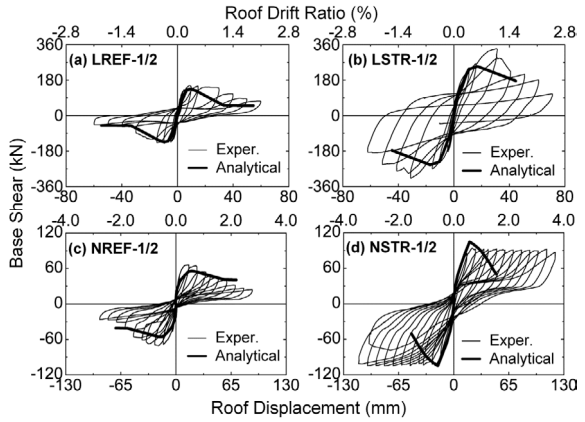

Fig. 9 Hysteretic base shear vs. roof displacement (drift ratio) curves.

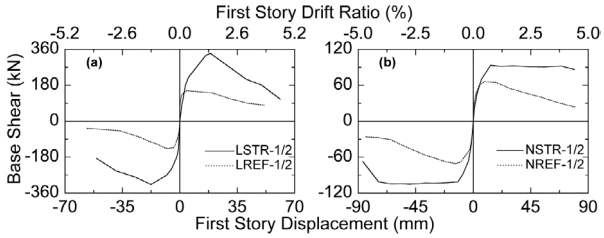

Fig. 10 Base shear vs. first story displacement envelope curves.

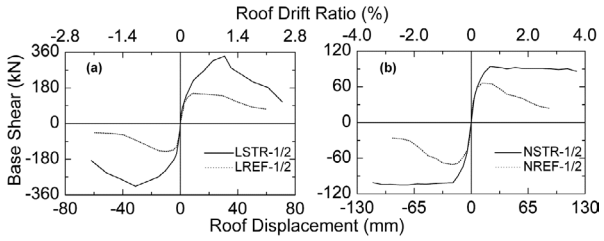

Fig. 11 Base shear vs. roof displacement envelope curves.

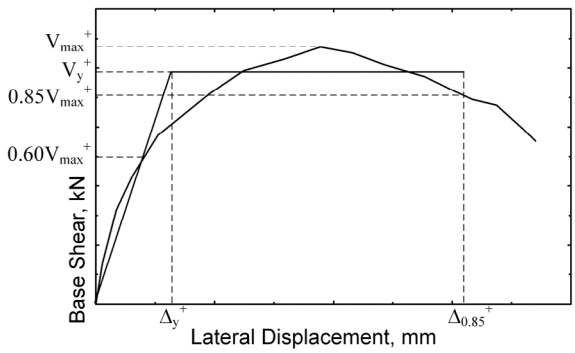

Fig. 12 Bi-linear approximation of envelope curves.

are obtained by tracing the peaks of each cycles of the hysteretic curves and illustrated in **Figs. 10** and **11** for the first story and the roof, respectively. In **Table 3**, the ultimate lateral load capacity (V_{max}), and initial stiffness (K) values are shown. The initial stiffness was computed as slope of the initial portion (i.e. the line that connects origin to ten percent of the ultimate load capacity on the ascending branch). The base shear vs. roof displacement envelope curves of the specimens (**Fig. 11**) were idealized based on an equal area concept presented in **Fig. 12**. The ultimate displacement ($\Delta_{0.85}$) was chosen to be the roof displacement corresponding to 15 percent decrease in the ultimate lateral load capacity. The displacement ductility of each specimen was estimated as the ratio of this ultimate roof displacement to the roof displacement corresponding to yield point of the idealized bi-linear envelope curves (i.e. Δ_y in **Fig. 12**). The roof displacements corresponding to yielding (Δ_y) and 15 percent decrease in the load capacity ($\Delta_{0.85}$), and displacement ductility of each specimen are also shown in **Table 3**.

The ratio of the ultimate lateral load capacity, initial stiffness and displacement ductility values of the strengthened specimens to the companion reference frames are presented in **Table 4**. The increments in the lateral load capacity provided by the applied strengthening were 2.23 and 1.42 in Series-L and Series-N, respectively. It may be concluded that the proposed CFRP strengthening assured a considerable enhancement in the lateral load carrying capacity of the RC frames with HCT infill walls in both test series. Yet, this was much more efficient in squat frames having lower aspect ratios, where strut and tie actions (i.e. evident by the deformations on HCT infill walls and diagonal CFRP sheets) were much more remarkable (Akın *et al*. 2011). The initial stiffness of 1/2 scaled RC frames was not altered significantly by the applied CFRP strengthening. The initial stiffness of specimen LSTR-1/2 was only about 20 percent higher than reference frame, LREF-1/2. And in case of Series-N, there was no change in the initial stiffness of frame as a result of strengthening.

In specimen LSTR-1/2, there was a sudden loss of strength after the ultimate capacity was reached due to anchorage failures and rupture of diagonal CFRP. Therefore, the displacement corresponding to 85 percent of the ultimate load capacity of LSTR-1/2 was low, which leads to less ductile response compared to LREF-1/2. On the other hand, the damage concentrated at the lap splice regions of NSTR-1/2 and HCT infill walls / diagonal CFRP sheets remained almost intact until end

Table 3 Test results of the specimens.

Spec.	V_y (kN)	V_{max} (kN)	Δ_y (mm)	Δ_{85} (mm)	K^+ (kN/mm)	Δ_{85}/Δ_y (%)	Failure Mechanism
LREF-1/2	144.0	152.4	4.5	34.0	40.0	7.6	Crushing of infill corners and wide shear cracks at beam-column joints
LSTR-1/2	305.0	339.8	11.2	40.0	47.0	3.6	Anchorage failure, de-bonding and rupture of CFRP sheets, wide shear cracks at beam-column joints
NREF-1/2	62.0	66.3	5.0	33.0	12.8	6.6	Plastic hinge formation at the bottom of first story columns
NSTR-1/2	89.0	94.0	9.5	120.0	13.3	12.6	Anchorage failure, de-bonding and rupture of CFRP sheets, plastic hinge formation at the bottom of first story columns

Table 4 The change in base shear capacity, initial stiffness and ductility provided by strengthening.

	$V_{max,STR}/V_{max,REF}$	K^+_{STR}/K^+_{REF}	$(\Delta_{85}/\Delta_y)_{STR}/(\Delta_{85}/\Delta_y)_{REF}$
Series-L	2.23	1.20	0.47
Series-N	1.42	1.04	1.91

of the test. This resulted in a base-rocking form of behavior and thus NSTR-1/2 continued to carry a significant portion of its lateral load capacity until the failure point (**Figs. 8d** and **9d**). Therefore, the displacement ductility of NSTR-1/2 was 91 percent higher when compared to specimen NREF-1/2.

The change in the energy dissipation characteristics of the test specimens with increasing lateral drift may be observed in **Fig. 13**. The energy dissipation in each cycle is estimated to be the area enclosed by the cyclic curve. It is clear that the applied strengthening increased the amount of energy that could be dissipated within the structure considerably in both series. In Series-L, the energy dissipation capacity of LSTR-1/2 was around three times that of specimen LREF-1/2, owing to the improved compression strut and tension tie actions provided by the CFRP strengthening. The energy dissipation capacity of strengthened frame in Series-N (i.e. NSTR-1/2) was 4.10 times higher than the non-strengthened reference specimen (i.e. NREF-1/2). However, this increment was observed along with the deformations which took place at the first story lap-splice regions and lead to a base-rocking type of behavior in NSTR-1/2. Since this type of behavior may lead to an instability for the whole structure, the higher increment of the dissipated energy in Series-N should be interpreted carefully.

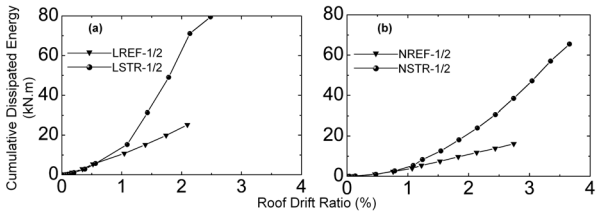

Fig. 13 Cumulative dissipated energy curves for (a) Series-L and (b) Series-N.

5. Scale effect

A structural model analysis should be utilized for the assessment of scale effect. The similitude relationships between the model (i.e. scaled structure) and prototype (i.e. actual structure) characteristics are defined in the structural model analysis. The similitude relationships that are used in this study are summarized below (Altın *et al*. 1990; Moncarz and Krawinkler 1981; Sabnis *et al*. 1983).

$$\text{Geometric similarity: } L_{\text{model}} = \lambda \times L_{prot.} \tag{1}$$

$$\text{Kinematic similarity: } \delta_{\text{model}} = n \times \delta_{prot.} \tag{2}$$

$$\text{Material similarity: } E_{\text{model}} = s \times E_{prot.} \tag{3}$$

In these relationships, L, δ, and E represent length, displacement and modulus of elasticity, respectively. λ, n and s are similitude constants that relate the model and prototype structures.

Besides, cross-sectional dimensions (b and h) and consequent moment of inertia (I) of the model and prototype structures may be related by use of geometric similarity relationship.

$$b_{\text{model}} = \lambda \times b_{prot.} \text{ and } h_{\text{model}} = \lambda \times h_{prot.} \tag{4}$$

$$I_{\text{model}} = \lambda^4 \times I_{prot.} \tag{5}$$

The shear force-displacement relationships of both model and prototype structures may be defined by using stiffness equations of structural analysis.

$$V_{\text{model}} = \frac{12 \times E_{\text{model}} \times I_{\text{model}}}{L_{\text{model}}^{\ 3}} \delta_{\text{model}} \tag{6}$$

$$V_{prot.} = \frac{12 \times E_{prot.} \times I_{prot.}}{L_{prot.}^{\ 3}} \delta_{prot.} \tag{7}$$

where V and δ represent the shear force and lateral displacement, respectively. After assuming λ=n and s=1 (i.e. same material for both prototype and model), the similitude relationship for the base shear may be derived by relating Eqns. 6 and 7.

Table 5 Prototype characteristics of 1/3 and 1/2-scaled test frames.

Test Group	Specimen	$V_{max,p}$* (kN)	$(V_{max,p})_{1/2}$ / $(V_{max,p})_{1/3}$	K^+_p* (kN/mm)	$(K^+_p)_{1/2}$ / $(K^+_p)_{1/3}$	Diss. Energy (DE_p)* (kN.m)	$(DE_p)_{1/2}$ / $(DE_p)_{1/3}$
Group-I (1/3-scaled)	LREF-1/3	630.0		150.0		166.3	
	LSTR-1/3	1098.0		201.0		531.4	
	NREF-1/3	228.6		37.8		126.4	
	NSTR-1/3	324.0		46.5		275.7	
Group-II (1/2-scaled)	LREF-1/2	609.6	1.0	80.0	0.5	201.8	1.2
	LSTR-1/2	1359.2	1.2	94.0	0.5	569.0	1.1
	NREF-1/2	265.2	1.2	25.6	0.7	129.0	1.0
	NSTR-1/2	376.0	1.2	26.6	0.6	377.4	1.4

*$V_{max,p}$, K^+_p and DE_p are the ultimate lateral load capacity, initial stiffness and total dissipated energy of the equivalent 1/1 scale prototype frame.

$$V_{\text{model}} = \lambda^2 \times V_{prot.} \tag{8}$$

The initial stiffness may be defined as any ratio of the base shear to lateral displacement (i.e. K=V/δ).

$$K_{\text{model}} = \lambda \times K_{prot.} \tag{9}$$

The dissipated energy is proportional to the applied force multiplied by the displacements. Therefore, similitude relationship for the dissipated energy may be obtained as:

$$DE_{\text{model}} = \lambda^3 \times DE_{prot.}$$

In this study, the set of 1/3 and 1/2-scaled specimens are termed as Group-I and Group-II specimens, respectively. The similitude constants for Group-I and Group-II frames are 1/3 and 1/2, respectively. Eventually, the similitude relationships of the ultimate lateral load (i.e. base shear capacity), initial stiffness and total dissipated energy may be shown as follows for Group-I and Group-II.

$$\begin{bmatrix} V_{prot.} = 9 \times V_{\text{model}} \\ K_{prot.} = 3 \times K_{\text{model}} \\ DE_{prot.} = 27 \times DE_{\text{model}} \end{bmatrix} \text{...(Group-I)} \tag{10}$$

$$\begin{bmatrix} V_{prot.} = 4 \times V_{\text{model}} \\ K_{prot.} = 2 \times K_{\text{model}} \\ DE_{prot.} = 8 \times DE_{\text{model}} \end{bmatrix} \text{...(Group-II)} \tag{11}$$

The ultimate lateral load, initial stiffness and dissipated energy of specimens in Group-I and Group-II are converted into characteristics of equivalent prototype frame (i.e. 1/1-scaled) and presented in **Table 5**. The ratio between prototype characteristics of equivalent 1/3 and 1/2-scaled frames are also given in the same table. In order to provide a more reliable comparison for the total amount of dissipated energy, the area enclosed by the hysteretic cycles up to the same roof drift ratio limit was considered for matching specimens in each scale group. This roof drift ratio limit was about 2.0 and 3.0 percent for Series-L and Series-N frames, respectively. Besides, the normalized base shear vs. roof displacement envelope curves of companion specimens in both test groups are presented together in **Fig. 14**. It should be noted that the experimental results of 1/3-scaled specimens are provided in the previous articles (Akın *et al*. 2011).

The results indicate that there may be no significant effect of scaling on the ultimate lateral load capacity attained by both non-strengthened and strengthened RC frames. This result seems to be valid for both test series with different aspect ratios. On the other hand, it may be

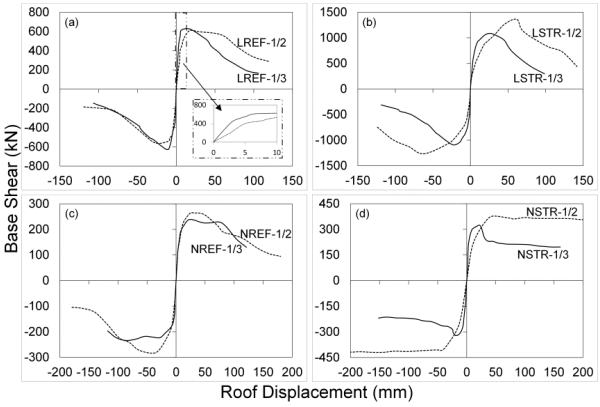

Fig. 14 Base shear vs. roof displacement envelope curves for equivalent prototype structures of 1/3- and 1/2-scaled test frames.

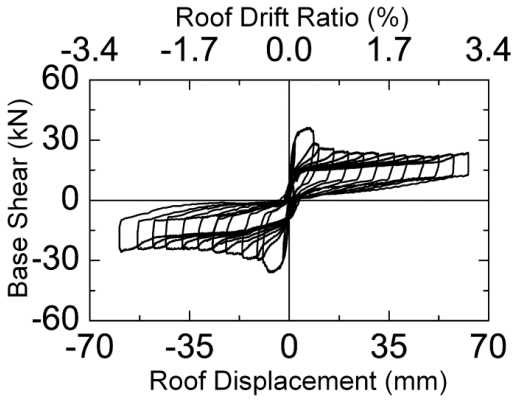

Fig. 15 Hysteretic base shear vs. roof displacement curve of NSTR-1/3 (i.e. 1/3-scaled).

stated that the post-peak behavior of RC test frames may be influenced considerably by scaling, which is explicit in **Fig. 14** (Bazant 1993). The energy dissipated by Series-L frames was slightly higher in case of 1/2-scaled group. The energy dissipation capacity of NSTR-1/2 was 40 percent higher in comparison to NSTR-1/3. Major part of this difference may be related to the sudden loss of strength in specimen NSTR-1/3, after ultimate lateral load capacity had been reached (**Figs. 14** and **15**). As explained by Akin *et al*. (2011), this strength loss may be caused by large bond-slip deformations at the lap-splice regions of first story columns. Nevertheless, the frame sustained significant amount of lateral displacements without another loss in strength. The effect of lap-splice deficiency resulted by large bond-slip deformations may be further studied in consideration of scale ratio.

The comparison of the equivalent prototype stiffness values of different scaled frames designates that the initial stiffness of smaller-scaled specimens is higher. The ratio between initial stiffness of 1/2 and 1/3-scaled frames is 0.5 in Series-L and approximately 0.65 in Series-N. It has been reported that the ultimate load level of concrete (i.e. quasi-brittle) structures is achieved when the cracks extend over about 50-90% of the cross-section (Bazant 1993). Considering larger cross-sectional dimensions in large scale specimens, it may be concluded that this should lead to higher lateral displacements experienced by the specimen before reaching ultimate load capacity. Besides, it is also known that observing a flaw becomes more probable in structural members, especially in case of concrete, as the size of the member increases (Silva and Rodrigues 2006). This phenomenon is also obvious in **Fig. 14**.

6. Numerical simulations

The two dimensional numerical models of the test frames were developed and non-linear pushover analyses were performed by using OpenSees software platform (Mazzoni *et al*. 2007). The modeling was carried out in the same manner as explained by Akin *et al*. (2011) and Akin *et al*. (2014) for 1/3-scaled test specimens. The non-linear beam-column element of OpenSees was utilized for RC frame members. The compressive forces exerted by the RC frame to the infill wall were assumed to be transferred along the diagonal of the wall with a constant width (i.e. compression strut). The CFRP sheets which were fixed along the reverse diagonal direction were assumed to act as tension tie, as they bear tensile stresses in this direction. The truss elements were used for the compression strut and tension tie. The Hognestadet al. (1955) and Kent and Park (1971) models were employed for the unconfined and confined concrete, respectively. The average concrete compressive strength of each test frame (given in **Table 1**) was used in the concrete models. The conventional uniaxial bi-linear steel model without strain hardening was used for the longitudinal reinforcement. The yield strength and elastic modulus values of the steel bars shown in **Table 2** were utilized in the analyses.

The lap-splice deficiency was mentioned to be effective on the failure of test specimens, especially in Series-N. Therefore, it is important to model the behavior of longitudinal steel bars at the lap-splice regions of columns. The axial tensile behavior of lapped longitudinal bars was predicted by using the effective steel stress approach proposed by Binici and Mosalam (2007). The details of this model were explained in the previous articles for 1/3-scaled test specimens (Akın *et al*. 2011; Akın *et al*. 2014). The model was originally developed for deformed bars and thus takes slip deformations of deformed bars into account. According to the best knowledge of authors, no model was available in order to represent the bond-slip behavior of lapped plain bars. Therefore, this model was modified with certain assumptions to approximate axial response of lapped plain bars. The confining effect that may be provided by both lateral steel and CFRP reinforcement was ignored for this purpose. A triangular bond stress distribution (i.e. zero stress at the free ends of longitudinal bars) was assumed in the model. And the force equilibrium of lapped bars under this bond stress distribution was constituted at any arbitrary level along the lap length. The level of force equilibrium was taken as the mid-height of lap-splice region, which yields minimum effective steel stress value. The model results in the effective stress-strain diagram shown in **Fig. 16** for the lapped longitudinal bars. In the same figure the constitutive steel model was also presented. The effective stress-strain diagram was idealized as a bi-linear curve with a yield tensile stress of 145 MPa.

The compression strut and tension tie models of Binici *et al*. (2007) were used in order to simulate the responses of HCT infill walls and diagonal CFRP sheets, respectively (Akın *et al*. 2011). These strut and tie models are illustrated in **Fig. 17**. The non-strengthened infill walls of the reference frames (i.e. LREF-1/2 and NREF-1/2) were modeled by using bi-linear strut models. On the other hand, CFRP strengthened infill walls were

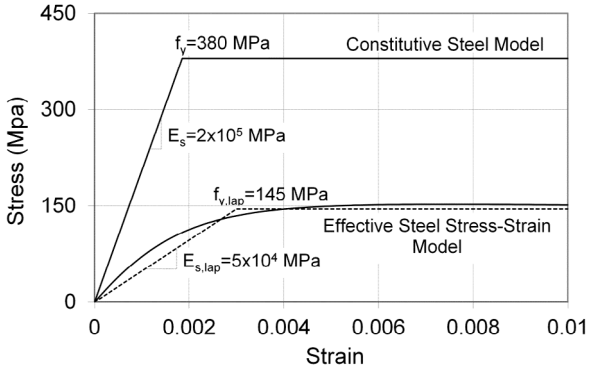

Fig. 16 Effective stress-strain model for lap splice regions of the columns.

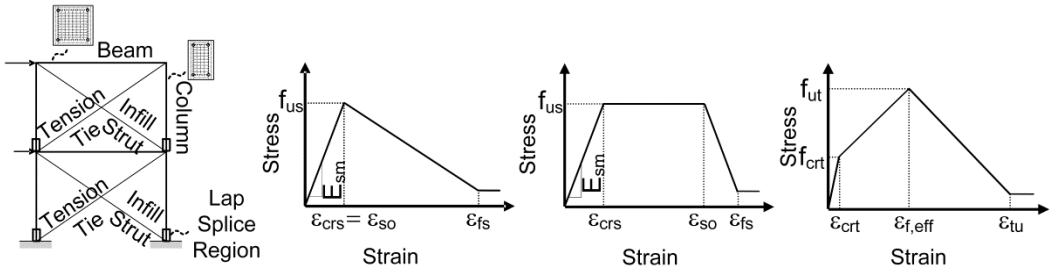

(a) Representative model of the strengthened frames (b) Strut model for non-strengthened infill walls (c) Strut model for strengthened infill walls (d) Tie model

Fig. 17 Modeling of the CFRP strengthened frames.

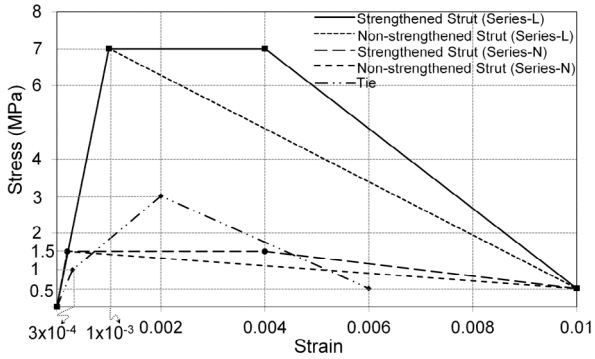

Fig. 18 Applied compression strut and tension tie models.

modeled by a ductile tri-linear model. The mechanical properties of mortar, infill unit, longitudinal steel and CFRP, which are provided in **Tables 1** and **2**, are utilized in the numerical model. The tensile strength of the plaster was assumed to be 0.5 MPa (i.e. approximately 10 percent of the compressive strength). The employed flexural capacity of the columns was estimated to be 12.0 kNm. The effective FRP strain ($\varepsilon_{f,eff}$), which depends on the failure modes of FRP, is effective both on strengthened strut and tie models. In the previous studies (Binici *et al*. 2007), effective FRP strain was recommended to be 0.002 and 0.004 for the anchorage failure and de-bonding of FRP, respectively. Same as in the numerical modeling of 1/3-scaled test frames, this strain value was taken as 0.002, since anchorage failure was observed especially in LSTR-1/2. The failure strain of FRP tie was proposed to be three times of the effective FRP strain (i.e. $\varepsilon_{tu}=3x\varepsilon_{f,eff}$) by the model (Binici *et al*. 2007). By referring to a study conducted by El-Dakhakhni *et al*. (2004), the failure strain of compression strut (ε_{fs}) was assumed to be 0.01 in the model. These strain values that define the failure states of both strut and tie were so used in the numerical models.

The resulting compression strut models corresponding to Series-L and Series-N frames are illustrated in **Fig. 18**. It should be noted that the tension tie model is independent of the aspect ratio of infill walls. Therefore, the same tie model was employed for both Series-L and Series-N (**Fig. 18**).

The analytical pushover curves of test specimens are presented in **Fig. 9** in conjunction with the corresponding experimental base shear-roof displacement curves. The comparison of the experimental and analytical ultimate lateral load and initial stiffness values is provided in **Table 6**. The estimation of the ultimate lateral load by the numerical model seems to match reasonable well with the experimental results. The initial stiffness values of Series-L specimens were, however, slightly underestimated by the model. On the other hand, the initial stiffness was overestimated by more than 20 percent in both frames of Series-N. This may be related to the bond-slip deformations experienced by the lapped longitudinal column bars. It was previously mentioned that the model (Binici and Mosalam 2007) was used with certain assumptions to represent lapped plain bars. The estimation of bond-slip deformations corresponding to plain bars may not be accurate enough with the available model that is for deformed bars. This further indicates a need for modeling bar slip behavior of lapped plain reinforcement.

The global drift characteristics of the analytical pushover curves and hysteretic test results of non-strengthened frames (i.e. LREF-1/2 and NREF-1/2) may be concluded to be reasonably close (**Figs. 9a** and **c**). On the other hand, the lateral drift response of strengthened specimens could not be predicted successfully by the numerical model in the post-elastic range of response (**Figs. 9b** and **d**). The effective CFRP strain may have considerable influence on this discrepancy. As

Table 6 Comparison of experimental and analytical results.

Specimen	Ultimate Lateral Load, V_{max} (kN)			Initial Stiffness, K^+ (kN/mm)		
	Expr.	Analy.	Analy./Expr.	Expr.	Analy.	Analy./Expr.
LREF-1/2	152.4	133.4	0.88	40.0	31.2	0.78
LSTR-1/2	339.8	248.6	0.73	47.0	41.7	0.89
NREF-1/2	66.3	55.6	0.84	12.8	15.4	1.20
NSTR-1/2	94	104.4	1.11	13.3	16.7	1.26

stated earlier, this strain value was assumed to be 0.002 that is recommended for the anchor failure mode (Binici *et al*. 2007), since this type of FRP failure had been observed during the experiments. The authors believe that, any assumption of the effective FRP strain higher than the value taken in this study may result in closer drift response in the post-elastic range.

7. Conclusions

The results of experimental and numerical studies that are carried out for CFRP strengthening of 1/2-scaled infilled RC frames are presented. In order to assess the scale effect, these results were further compared with the previous test results of matching 1/3-scaled RC frames. The possible conclusions are summarized below. Any additional inference on these results should be drawn carefully and generalization without due reasoning should be avoided.

- The lateral load and energy dissipation capacities of 1/2-scaled RC frames with infill walls were increased significantly by the applied CFRP strengthening. These enhancements in response were higher in case of shear dominant Series-L frames.
- There was a sudden loss of strength that was triggered by anchorage failures and rupture of diagonal sheets in strengthened squat frames which, on the other hand, attained superior lateral load levels. This resulted in a less ductile behavior in the post-elastic range of response in comparison to the non-strengthened frame. This was not the case in Series-N frames where strut and tie actions were not as efficient as Series-L.
- There was only a slight increase in the initial stiffness of Series-L frames as a result of CFRP strengthening. Yet, there was no alteration of initial stiffness in Series-N frames by the applied rehabilitation.
- There may be no considerable effect of specimen scaling on the ultimate lateral load capacity of both non-strengthened and strengthened RC frames.
- The energy dissipated by 1/2-scaled specimens is slightly higher in comparison to the 1/3-scaled frames in both series of aspect ratio. Since the ultimate lateral load levels are similar for both scale groups, this should be related with the improved drift characteristics of 1/2-scaled frames in the plastic deformation range.
- The initial stiffness of 1/2-scaled frames were approximately 50 and 65 percent those of 1/3-scaled specimens, in case of Series-L and Series-N, respectively. The higher probability of observing defects in large-scaled concrete members may lead to a more widespread cracking and lower stiffness values.
- The ultimate lateral load and initial stiffness of test frames were calculated approximately close by the numerical model that was employed in this study. The initial stiffness was overestimated by about 20 percent by the numerical model in Series-N. This may be related to the use of bond-slip model that was originally developed for deformed bars. In case of narrow frames where lap-splice deficiency becomes critical, this model may not represent the bar slip response of lapped plain bars. Therefore, a bond-slip model for lapped plain bars may be required especially for modeling older buildings which has this deficiency.
- The lateral drift characteristics of analytical pushover curves were reasonably close to those of experimental hysteretic curves in both of the non-strengthened frames. On the other hand, the numerical model was not successful in predicting the lateral drift response of strengthened frames in both test series. The effective CFRP strain is the major parameter in terms of designating the post-elastic strain capacity of both strut and tie models in strengthened frames. Therefore, the strain levels endured by the diagonal CFRP sheets, which might be higher than the assumed effective CFRP strain (i.e. same as in 1/3-scaled specimens) may induce such a difference. The numerical model may thus be scale sensitive on account of the experienced CFRP strain level.

Acknowledgements

The experimental part of this study was conducted at METU Structural Mechanics Laboratory with the financial support of BAP (Grant No. BAP-08-11-DPT-2002K120510).

References

ACI Committee 318, (2005). "*Building code requirements for structural concrete (ACI 318-05) and commentary* (ACI 318R-05)." American Concrete Institute, Farmington Hills, MI, 2005, 430 p.

Almusallam, T. H. and Al-Salloum Y. A., (2007). "Behavior of FRP strengthened infill walls under in-plane seismic loading." *Journal of Composites for Construction*, ASCE, 11(3), 308-318.

Akın, E., Canbay, E., Binici, B. and Özcebe, G., (2011). "Testing and analysis of infilled reinforced concrete frames strengthened with CFRP reinforcement." *Journal of Reinforced Plastics and Composites*, 30(19), 1605-1620.

Akın, E., Özcebe, G., Canbay, E. and Binici, B., (2014). "Numerical study on CFRP strengthening of reinforced concrete frames with masonry infill walls." *Journal of Composites for Construction,* ASCE, 18(2),

Altın, S., (1990). "*Strengthening of reinforced concrete frames with reinforced concrete infills*." PhD Thesis, Middle East Technical University, Ankara, 350 p.

Bazant, Z., (1993). "Scaling laws in mechanics of failure." *Journal of Engineering Mechanics*, ASCE, 119(9), September, 1828-1844.

Binici, B. and Mosalam, Khalid M., (2007). "Analysis of reinforced concrete columns retrofitted with fiber reinforced polymer lamina." *Composites B: Engineering*, 38(2), 265-276.

Binici, B., Özcebe, G. and Özçelik, R., (2007).

"Analysis and design of FRP composites for seismic retrofit of infill walls in reinforced concrete frames." *Composites B: Engineering*, 38(5-6), 575-583.

El-Dakhakhni, W., Hamid, A. and Elgaaly, M., (2004). "Seismic retrofit of concrete-masonry-infilled steel frames with glass fiber-reinforced polymer laminates", *Journal of Structural Engineering*, ASCE, 130(9), 1343-1352.

Erol, G., Karadoğan, H. F. and Çılı, F., (2008). "Seismic strengthening of infilled RC frames by CFRP." *Proceedings of 14th World Conference on Earthquake Engineering*, October 12-17, Beijing, China.

Ersoy, U., Özcebe, G., Tankut, T., Akyüz, U., Erduran, E. and Erdem, İ., (2003). "Strengthening of infilled walls with CFRP sheets." *Seismic Assessment and Rehabilitation of Existing Buildings*, NATO Science Series, 29, 305-334.

Hognestad, E., Hanson, N. W. and McHenry, D., (1955). "Concrete stress distribution in ultimate strength design." *Journal of American Concrete Inst.*, 52(4), 455-477.

Kent, D. C. and Park, R., (1971). "Flexural members with confined concrete", *Journal of Structural Engineering*, ASCE, 97(7), 1969-1990.

Kobayashi, K., (2007). "Innovative application of FRP's to seismic retrofit of brick-infilled RC frames." *Proc. FRPRCS-8*, Univ. of Patras, Patras, Greece.

Luccioni, B. and Rougier, V. C., (2011). "In-plane retrofitting of masonry panels with fibre reinforced composite materials." *Construction and Building Materials*, 25(4), 1772-1788.

Mahmood, H. and Ingham, J. M., (2011). "Diagonal compression testing of FRP-retrofitted unreinforced clay brick masonry wallettes." *Journal of Composites for Construction*, ASCE, 15(5), 810-820.

Mazzoni, S., McKenna, F., Scott, M. H. and Fenves, G. L., (2007). "*Open system for earthquake engineering simulation (OpenSees) user command-language manual*." Version 2.0, Univ. of California, Berkeley, CA, <http://opensees.berkeley.edu./OpenSees/manuals/usermanual/> [Accessed June 2013].

Moncarz, P. D. And Krawinkler, H., (1981). "*Theory and application of experimental model analysis in earthquake engineering*." Report No. 50, Dept. Of Civil Eng., Stanford University, Stanford, CA, 263 p.

Nateghi-Elahi, F. and Dehghani, A., (2008). "Analytical and numerical study of RC frames with URM infilled retrofitted by CFRP." *Proceedings of 14th World Conference on Earthquake Engineering*, October 12-17, Beijing, China.

Özcebe, G., Ersoy, U., Tankut, T., Akyüz, U. and Erduran, E., (2004). "Rehabilitation of existing reinforced concrete structures using CFRP fabrics." *Proceedings of 13th World Conference on Earthquake Engineering*, August 1-6, Vancouver, B.C., Canada.

Özcebe, G., Binici B., Ersoy, U., Tankut, T., Özden, Ş., Karadoğan, H. F., Yüksel, E. and İlki, A., (2006). "*Analysis of infilled reinforced concrete frames strengthened with FRP's*." Retrofitting of Concrete Structures by Externally Bonded FRP's, FIB, Technical Report, International Federation for Structural Concrete (fib), Lausanne, Switzerland, 167-197.

Özden, Ş. and Akgüzel, U., (2006). "CFRP overlays in strengthening of frames with column rebar lap splice problem." *Advances in Earthquake Engineering for Urban Risk Reduction*, NATO Science Series: IV: Earth and Environmental Sciences, 66, 275-284.

Saatcioglu, M., Serrato, F. and Foo, S., (2005). "Seismic performance of masonry infill walls retrofitted with CFRP sheets." *ACI-SP230: 7th Int. Symp. on Fiber-Reinforced Polymer (FRP) Reinforcement for Concrete Structures*, American Concrete Institute (ACI), MI, 341-354.

Sabnis, G. M., Harris, H. G., White, R. N. and Mirza, M. S., (1983). "*Structural modeling and experimental techniques*." Prentice-Hall, Englewood Cliffs, N.J., 585 p.

Silva, M. A. G. And Rodrigues, C. C., (2006). "Size and relative stiffness effects on compressive failure of concrete columns wrapped with glass FRP." *Journal of Materials in Civil Engineering*, ASCE, 18(3), 334-342.

Spyrakos, C. C., Maniatakis, C. A., Smyrou, E. and Psycharis, I. N., (2012). "FRP strengthened brick-infilled RC frames: An approach for their proper consideration in design." *The Open Construction and Building Technology Journal*, 6 (Spec. Iss. 1), 306-324.

Tan, M., Binici, B. and Özcebe, G., (2009). "Seismic strengthening of a mid-rise reinforced concrete frame using CFRP's: a real life application." *Proceedings of 9th International Symposium on Fiber Reinforced Polymer Reinforcement for Concrete Structures* (FRPRCS-9), July 13-15, University of Adelaide, Adelaide, Australia.

Turkish Earthquake Code, (2007). "*Turkish code for buildings in seismic zones*." Ministry of Public Works and Settlement, Turkey, 159 p.

Yüksel, E., İlki, A., Erol, G., Demir, C. and Karadogan, H. F., (2006). "Seismic retrofit of infilled reinforced concrete frames with CFRP composites." *Advances in Earthquake Engineering for Urban Risk Reduction*, NATO Science Series: IV: Earth and Environmental Sciences, 66, 285-300.

Yüksel, E., Özkaynak, H., Büyüköztürk, O. and Yalçın, C., (2009). "Performance of alternative CFRP retrofitting schemes used in infilled RC frames." *Construction and Building Materials*, 24(4), 596-609.